HHS Public Access

Author manuscript

Cell Physiol Biochem. Author manuscript; available in PMC 2023 May 09.

Published in final edited form as:

Cell Physiol Biochem. 2021 August 20; 55(4): 489–504. doi:10.33594/000000400.

Nox4 knockout does not prevent diaphragm atrophy, contractile dysfunction, or mitochondrial maladaptation in the early phase post-myocardial infarction in mice

Dongwoo Hahn[1], **Ravi A. Kumar**[1], **Derek R. Muscato**[1], **Terence E. Ryan**[1], **Katrin Schröder**[2], **Leonardo F. Ferreira, PhD**[1]

[1]Department of Applied Physiology and Kinesiology, College of Health and Human Performance, University of Florida, Gainesville, FL

[2]Institute for Cardiovascular Physiology, Goethe University, Frankfurt, Germany

Abstract

Background: Diaphragm dysfunction with increased reactive oxygen species (ROS) occurs within 72 hrs post-myocardial infarction (MI) in mice and may contribute to loss of inspiratory maximal pressure and endurance in patients.

Methods: We used wild-type (WT) and whole-body Nox4 knockout (Nox4KO) mice to measure diaphragm bundle force *in vitro* with a force transducer, mitochondrial respiration in isolated fiber bundles with an O_2 sensor, mitochondrial ROS by fluorescence, mRNA (RT-PCR) and protein (immunoblot), and fiber size by histology 72 hrs post-MI.

Results: MI decreased diaphragm fiber cross-sectional area (CSA) (~15%, $p = 0.015$) and maximal specific force (10%, $p = 0.005$), and increased actin carbonylation (5–10%, $p = 0.007$) in both WT and Nox4KO. Interestingly, MI did not affect diaphragm mRNA abundance of MAFbx/atrogin-1 and MuRF-1 but decreased Nox4KO decreased it by 20–50% ($p < 0.01$). Regarding the mitochondria, MI and Nox4KO decreased the protein abundance of citrate synthase and subunits of electron transport system (ETS) complexes and increased mitochondrial O_2 flux (JO_2) and H_2O_2 emission (JH_2O_2) normalized to citrate synthase. Mitochondrial electron leak (JH_2O_2/JO_2) in the presence of ADP was lower in Nox4KO and not changed by MI.

Conclusions: Our study shows that the early phase post-MI causes diaphragm atrophy, contractile dysfunction, sarcomeric actin oxidation, and decreases citrate synthase and subunits of mitochondrial ETS complexes. These factors are potential causes of loss of inspiratory muscle

Corresponding author: Leonardo F. Ferreira, PhD, Department of Applied Physiology and Kinesiology, University of Florida, 1864 Stadium Rd, room 100 FLG, Gainesville, FL, 32611-8205, ferreira@hhp.ufl.edu, +1-352-294-1724.

Author contributions

Designed the study and experiments: DH, TER, LFF; Performed experiments: DH, RAK, DRM, LFF; Data analysis and interpretation: DH, RAK, DRM, TER, KS, LFF; Provided essential resources: TER, KS, LFF; Drafted and edited the manuscript: DH, RAK, TER, KS, LFF; Aproved the manuscript: DH, RAK, DRM, TER, KS, LFF.

Statement of Ethics

Our animal experiments conformed to internationally accepted standards and have been approved by the University of Florida Institutional Animal Care and Use Committee protocol 201809075.

Disclosure Statement

The authors have no conflict of interest.

strength and endurance in patients, which likely contribute to the pathophysiology in the early phase post-MI. Whole-body Nox4KO did not prevent the diaphragm abnormalities induced 72 hrs post-MI, suggesting that systemic pharmacological inhibition of Nox4 will not benefit patients in the early phase post-MI.

Keywords

atrophy; oxidants; force; respiration; heart failure

Introduction

Myocardial infarction (MI) is one of the most common forms of pathology in the heart and results in cardiomyocyte dysfunction and death due to ischemia (24). The primary concerns in the care of patients in the early phase post-MI are cardiac revascularization and arrhythmias. However, recent studies in patients and rodents identified that the early phase post-MI is accompanied by inspiratory muscle (diaphragm) weakness and endurance (7, 39, 50), which bears relevance to the overall cardiopulmonary pathophysiology (27). Diaphragm abnormalities contribute to dyspnea (60), impaired airway clearance (49), and elevated sympathetic nervous activity (15) – the latter is a critical determinant of arrhythmias post-MI (17, 31) that can lead to cardiac arrest and death (14, 15).

The early phase post-MI is characterized by elevated circulating inflammatory cytokines and angiotensin II (30, 33), which signal via reactive oxygen species (ROS) (7, 26). Excess ROS causes muscle weakness due to atrophy and contractile dysfunction (12, 55) and impairs mitochondrial function (20). A potential source of ROS downstream of inflammatory cytokines and angiotensin II is NADPH oxidase 4 (Nox4) (32, 61). Nox4, which localizes in the sarcoplasmic reticulum and mitochondria (2, 46, 52), causes skeletal muscle atrophy induced by angiotensin II infusion and pancreatic cancer (13, 26), mediates contractile dysfunction in metastatic bone cancer (57), and promotes mitochondrial dysfunction (2). In the early phase post-MI, the systemic environment is primed to activate Nox4 signaling (13, 37, 51). However, the role of Nox4 on diaphragm atrophy, contractile dysfunction, and potential mitochondrial abnormalities in the early phase post-MI is unknown.

The main goal of this study was to test the role of Nox4 on diaphragm weakness in the early phase post-MI. Based on the localization of Nox4 in mitochondria (46) and the relevance of mitochondrial function to muscle health in several conditions (23), we aimed to define the impact of MI on diaphragm mitochondrial respiration and ROS emission and the role of Nox4 therein.

Methods

Animals and ethical approval

We conducted experiments on 7–9 months old male mice: twelve C57BL/6J (WT; Jackson Laboratories) and thirteen whole-body Nox4 knockout (Nox4KO; a gift from Drs. Ralf Brandes and Katrin Schröder). Nox4 knockout mice were generated by targeted deletion of the translation initiation site and exons 1 and 2 of the gene as described previously

(63). We backcrossed the original litter of Nox4KO with C57BL/6J for over ten generations and confirmed the genotype of all Nox4KO mice used in this study (Figure S1) following a previous protocol (47). We housed the mice at the University of Florida Animal Care Facilities in a 12:12-h light-dark cycle and supplied standard chow and water *ad libitum*. We followed guidelines set by the National Institutes of Health for all animal procedures performed in this study. The protocol was approved by the Institutional Animal Care and Use Committee of the University of Florida.

Coronary artery ligation

Animals went through ligation of the coronary artery to cause myocardial infarction using aseptic procedures or sham surgery. We anesthetized the animals with a mixture of isoflurane (3–5% for induction, 2–3% for maintenance) and oxygen, shaved the left side of the thorax, and cleaned the surgical area with 4% chlorhexidine gluconate and sterile saline. When animals reached the surgical plane of anesthesia, we performed orotracheal intubation and connected the animal to a rodent respirator (Model 683, Harvard Apparatus Inc. Holliston, MA). We made incisions through the skin using a scalpel blade and bluntly dissected the thoracic muscle layer and intercostal muscles to expose the heart. Once the heart was exposed, we removed the pericardium and ligated the left anterior descending coronary artery close to the left atrium with a 6–0 monofilament absorbable PGA suture (DemeSORB™, DemeTECH, Miami Lakes, FL). After the ligation, we hyperinflated the lungs and closed the chest wall (6–0 PGA suture, DemeSORB™, DemeTECH) and skin (3–0 Nylon, Demelon™, DemeTECH). The animals in the sham group went through the same procedure except for the coronary artery ligation. We injected buprenorphine SR-LAB (ZooPharm, Laramie, WY) subcutaneously (1.0 mg/kg) immediately before surgery for analgesia. We supplied moist chow at the bottom of the cage and kept the cage for three days on top of a water-heated pad (Stryker, Kalamazoo, MI) to maintain the temperature of the cage at ~32°C.

Terminal experiments

We performed terminal experiments 72 hrs post-surgery. After we anesthetized the animal with isoflurane (5% induction, 2–3% maintenance), we performed laparotomy to collect the whole diaphragm and heart. We used the left hemidiaphragm to assess contractile function and the right hemidiaphragm for mitochondrial assays with saponin-permeabilized muscle fiber bundles. The unused portions of the diaphragm were snap-frozen in liquid nitrogen or embedded in Tissue-Tek OCT freezing medium (Sakura Finetek, Torrance, CA), frozen in liquid nitrogen-cooled isopentane, and stored at −80°C. We measured the weight of the heart after removing the atria and saved it in Tissue-Tek OCT freezing medium following the procedures described above for the diaphragm.

Histology

We used a cryostat (CM 3050S, Leica, Biosystems, Buffalo Grove, IL) set at −20°C to collect 10 μm cross-sections of the diaphragm and heart samples frozen in Tissue-Tek OCT freezing medium (Sakura Finetek, Torrance, CA). After transferring sections to the microscope slides, we covered the sections with wheat germ agglutinin (WGA) Texas Red (Molecular Probes, Eugene, OR) diluted in 1:200 at room temperature (15 min for heart,

1 hr for diaphragm). We washed the sections in phosphate-buffered saline (PBS) for 3 × 5 min, allowed them to dry, and followed different approaches for heart and diaphragm sections. For heart sections, we made panoramic images using an inverted microscope (Axio Observer, Zeiss, Thornwood, NY) connected to a camera (AxioCam ERc5s) and Zen Pro software (Zeiss Thornwood, NY). The percentage infarct size was the average percentage of endocardial and epicardial infarct length. We used this approach as WGA lectin binds to N-acetylglycosamin, which is rich in the extracellular matrix and connective tissue in the scar of the infarcted area (18).

For the diaphragm, we permeabilized the sample (after WGA staining and washes) with 0.5% Triton X-100 solution for 5 min, washed in PBS for 5 min, and incubated in primary antibodies in a humid chamber for 1.5 hrs. We used primary antibodies for myosin heavy chain type I (A4.840, 1:15; Developmental Studies Hybridoma Bank, Iowa City, IA) and type IIa (SC-71, 1:50, Developmental Studies Hybridoma Bank, Iowa City, IA). Subsequently, we washed the sample in PBS for 3 × 5 min and incubated it with fluorescently conjugated secondary antibodies (Goat × Mouse IgM Alexa 350 and Goat × Mouse IgG Alexa 488, Invitrogen, Carlsbad, CA) for 1 hr. We washed the sectioned tissue in PBS for 3 × 5 min and allowed it to dry. Lastly, we imaged the sections using an inverted fluorescence microscope (Axio Observer, Zeiss, Thornwood, NY) connected to a fluorescence camera (AxioCam MRm, Zeiss, Thornwood, NY) and Zen Pro software (Zeiss, Thornwood, NY). We used an automated image quantification platform to analyze fiber type distribution and cross-sectional area (MyoVision, University of Kentucky College of Health Sciences, Lexington, KY) (59).

qPCR

We retrieved diaphragm samples from Tissue-Tek OCT freezing medium (Sakura Finetek, Torrance, CA) in sterile PBS and homogenized them in TRI-Reagent (Sigma Aldrich, St. Louis, MO) using stainless steel beads and a bullet blender (Next Advanced, Troy, NY). We isolated RNA by using the Direct-Zol RNA Microprep kit (Zymo Research, Irvine, CA). We assessed RNA quantity and quality with UV spectroscopy (Thermo Fisher, Waltham, MA), then generated cDNA using the Quantabio qScript cDNA synthesis kit (Quantabio, Beverly, MA). Real-time PCR was performed on a Quantstudio 3 thermocycler (Thermo Fisher, Waltham, MA) using Taqman Universal Master Mix II and Taqman probes (all from Thermo Fisher, Waltham, MA) for *Nox4* (Mm00479246_m1), *Fbxo32* (Mm00499523_m1; MAFbx/atrogin-1), and *Trim63* (Mm01185221_m1; MuRF-1). Results were normalized to *HPRT* (Mm00446968_m1) and gene expression was calculated relative to the WT-Sham group using the ΔΔCT method.

Diaphragm contractile function in vitro

We immersed the left hemidiaphragm in bicarbonate buffered solution (in mM: 137 NaCl, 5 KCl, 1 $MgSO_4$, 1 NaH_2PO_4, 24 $NaHCO_3$, 2 $CaCl_2$) bubbled with a mixture of 95% O_2 and 5% CO_2 gas at room temperature and isolated a strip with ribs and central tendon attached to it. We tied the rib to a glass rod (158816; Radnoti, Monrovia, CA) and attached the central tendon to a Dual-Mode Muscle Lever System (300C-LR, Aurora Scientific Inc., Aurora, Canada) with 4–0 silk suture (Fine Scientific, Foster City, CA). We kept the bundle between

platinum electrodes connected to a biphasic high-power stimulator (701C, Aurora Scientific Inc., Aurora, Canada) in a water-jacketed organ bath filled with Krebs buffer continuously bubbled with 95% O_2 and 5% CO_2 gas. We found the optimal length of the bundle (L_0) by measuring tetanic force in response to 120 Hz stimulation (600 mA current, 0.25 ms pulse) at room temperature. After we placed the bundle at L_0, we increased the temperature of the organ bath and allowed 10 min for thermo-equilibration at 37°C, and stimulated at frequencies of 1, 30, 50, and 300 Hz.

After the protocol, we retrieved the diaphragm bundle from the apparatus, blotted it dry, and measured the bundle weight. We calculated the diaphragm bundle cross-sectional area (CSA, cm^2) based on the wet weight (g) and estimated muscle density (1.056 g/cm^3) (8) to determine the specific force (N/cm^2). We used the 'high throughput' function of DMA software (Aurora Scientific, Aurora, Canada) to analyze isometric contractile properties.

Muscle bundle preparation for mitochondrial function assessment

Our optimized approach to prep the mouse diaphragm for saponin-permeabilization of fiber bundles has been described in detail recently (22). Briefly, we placed the diaphragm sample in fresh ice-cold buffer X (in mM: 7.23 K_2EGTA, 2.77 Ca-K_2EGTA, 20 imidazole, 20 taurine, 5.7 ATP, 14.3 PCr, 6.56 $MgCl_2$-$6H_2O$, 50 K-MES; pH 7.1) in a tissue culture dish with silicone gel. After removing the ribs, blood clots, adipose and connective tissues, we cut the diaphragm perpendicular to the fiber orientation along the phrenic nerve and peeled off the abdominal fascia and muscle fiber layer. We used the 'pleural layer' of diaphragm fibers for bundle preparation, as this side contains a thinner fascia and less connective tissue than the abdominal side (48). We teased individual fibers longitudinally and left 0.1–0.2 mm of the fibers attached at the end of the bundle to prevent losing fibers during washing and transfer between containers. We trimmed the distal end of the separated fibers to remove portions potentially damaged during the teasing process. We transferred the separated bundles to microcentrifuge tubes with 1.5 ml of buffer X + saponin (30 μg/ml), and rotated the tubes for 30 min at 4°C. Lastly, we washed the bundles for 3 × 5 min at 4°C in a microcentrifuge tube with 1.5 ml buffer Z (in mM: 30 KCl, 10 KH_2PO_4, 5 $MgCl_2$-$6H_2O$, 105 K-MES, and 0.5 mg/ml BSA; pH 7.1). The individual bundles were then allocated to measurements of mitochondrial respiration (2 bundles) and ROS emission (1 bundle).

Mitochondrial respiration

We measured O_2 consumption at 37°C in buffer Z containing 20 mM creatine monohydrate and 10 μM blebbistatin (41) in a high-resolution respirometer (O2K Oxygraph; Oroboros, Innsbruck, Austria). We used Hamilton Syringes (Hamilton, Reno, NV) to add substrates and cytochrome c in the following order: 5 mM pyruvate + 0.5 mM malate (State 2 respiration, complex I), ADP (100 μM, 500 μM; State 3 respiration, complex I), 10 mM cytochrome c (mitochondrial membrane integrity), and 10 mM succinate (State 3 respiration, complex I+II). We initiated the experiment when the O_2 concentration of the buffer was stabilized at approximately 400 μM, and reoxygenated the buffer when O_2 concentration was less than 250 μM during the protocol. Once we finished the measurements, we retrieved the bundles to quantify the total protein content of the bundles

(DC Assay, Bio-Rad Laboratories, Hercules, CA). We completed the experiments in two bundles per mouse and used the average JO_2 for data analysis. We excluded bundles that displayed a JO_2 increase ≥ 10% upon addition of cytochrome c from analysis (2 bundles from separate animals within WT-MI, 1 bundle from Nox4KO-MI). The bundles used for mitochondrial respiration were retrieved from the O2K chamber, blotted dry, transferred to a microcentrifuge tube, snap-frozen in liquid nitrogen, and stored at −80°C. For measurement of total protein content in permeabilized bundles, we added 50 μl of mitochondrial isolation medium to the microcentrifuge tube, homogenized the samples in the microcentrifuge tube using a motor-driven polypropylene micropestle, centrifuged the homogenate at 500 g for 7 min at 4°C (#5424 Eppendorf, Hauppauge, NY), and used the supernatant for measurement of total protein content (DC Assay, Bio-Rad Laboratories, Hercules, CA). The JO_2 data were normalized to total protein per bundle and citrate synthase abundance to estimate intrinsic mitochondrial respiratory function (29).

Mitochondrial reactive oxygen species emission

We used an assay based on Amplex Ultra Red (Life Technologies, Eugene, OR) fluorescence (λ_{Em} = 565 nm, λ_{Exc} = 600 nm) to measure H_2O_2 emission from permeabilized diaphragm fiber bundles in a fluorometer (Fluorolog-3, Horiba Jobin Yvon Inc., Edison, NJ) with a 1 ml quartz cuvette (14-958-109, Fisherbrand, Pittsburgh, PA) maintained at 37°C. The assay solution contained 10 μM Amplex Ultra Red, 25 μM blebbistatin, 20 mM creatine monohydrate, 30 mM KCl, 10 mM KH_2PO_4, 5 mM $MgCl_2$-$6H_2O$, 8 μM BSA, 105 mM K-MES, 1 mM EGTA; pH 7.1, 30 U/ml superoxide dismutase, and 1 U/ml horseradish peroxidase. Initially, we allowed a 5-min period for thermal equilibration and stabilization of the fluorescence signal. Subsequently, we measured H_2O_2 emission rates from the permeabilized fiber bundles at baseline and after stepwise addition of substrates as in the mitochondrial respiration experiment. Once we finished the measurements, we retrieved the bundle to determine the total protein content of the bundles as described for mitochondrial respiration. Before each round of the experiment, we defined a standard curve for the relationship between Amplex Ultra Red fluorescence and [H_2O_2], converted fluorescence values to [H_2O_2], and subtracted baseline H_2O_2 rate to obtain the substrate-induced H_2O_2 flux, JH_2O_2. We calculated the $JH_2O_2/JO_2 \times 100$ under matching conditions of JH_2O_2 and JO_2 measurements to determine the percentage mitochondrial ETS electron leak.

SDS-PAGE and immunoblotting

We homogenized the diaphragm samples using a Kontess Duall Homogenizer in mitochondrial isolation medium (in mM: sucrose 300, Tris 10, EGTA 1; pH 7.1), centrifuged the homogenate at 500 g for 7 min at 4°C (#5424 Eppendorf, Hauppauge, NY) and saved the supernatant for measurement of total protein content (DC Assay, Bio-Rad Laboratories, Hercules, CA) and SDS-PAGE and immunoblotting. We mixed the supernatant 1:3 with 4× Laemmli buffer (Bio-Rad Laboratories, Hercules, CA) with 0.35 M dithiothreitol, loaded approximately 15 μg of protein per lane into 4–20% Criterion™ TGX™ stain-free gels (Bio-Rad Laboratories, Hercules, CA), and ran electrophoresis for 50 min at 200 V with the apparatus surrounded by ice. We activated and scanned the gel in a Gel Doc EZ Imager (Bio-Rad Laboratories, Hercules, CA) and determined the total protein in each lane (Image

Lab, Bio-Rad Laboratories, Hercules, CA). Subsequently, we transferred the proteins to a nitrocellulose membrane (GE Healthcare Life Sciences, Pittsburgh, PA) at a constant current (100 mA) overnight at 4°C. We blocked the membrane with Odyssey Blocking Buffer (LI-COR, Lincoln, NE) for 1 hr at room temperature. Then, we washed the membrane with Tris-buffered solution (TBS) for 5 min and incubated it with primary antibody for citrate synthase (ab96600; Abcam, Cambridge, MA) at 1:1,000 dilution and total OXPHOS antibody cocktail (ab110413; Abcam, Cambridge, MA) at 1:1,000 dilution for 1 hr at room temperature to detect citrate synthase and mitochondrial complexes I-V. Thereafter, we washed the membrane with TBS containing 0.1% of TWEEN®−20 (Sigma-Aldrich, St. Louis, MO) 4 × 5 min, followed by a TBS rinse for 5 min. We then incubated the membrane with secondary antibodies $IRDye_{680}$ (926–68020; LI-COR, Lincoln, NE) at 1:40,000 dilution and $IRDye_{800}$ (926–32211; LI-COR, Lincoln, NE) at 1:20,000 dilution for 1 hr in the dark, followed by a rinse as described above. We scanned the membrane in Odyssey CLx Infrared Imaging System (LI-COR, Lincoln, NE) and used Image Studio Lite Software (Li-COR, Lincoln, NE) to quantify the optical density of specific bands. We normalized the signal for each target protein to the total protein per lane, which were all within the linearity of the assays. We did not measure Nox4 protein abundance because there was no commercial antibody that reliably detected Nox4 – all antibodies tested showed a protein band in knockout animals, despite confirmed genotype and undetectable Nox4 mRNA.

For determination of myosin heavy chain and actin abundance and actin carbonylation, we homogenized the diaphragm samples in ice-cold high-salt protein isolation buffer (in mM: 300 NaCl, 100 NaH_2PO_4, 50 Na_2HPO_4, 10 $Na_4P_2O_7$, 1 $MgCl_2$, 10 EDTA, 1 dithiothreitol; pH 7.1) (10, 44) containing Halt protease inhibitor cocktail (Thermo Scientific, Waltham, MA). After homogenization, we centrifuged the samples at 10,000 g for 3 min at 4°C and used the supernatant for the assays. We measured total protein content with a Bradford assay (23246; Thermo Fisher Scientific, Waltham, MA), diluted the samples to similar protein contents, and mixed 1:1 with 2× Laemmli buffer (Bio-Rad Laboratories, Hercules, CA) containing 0.35 M dithiothreitol and heat-denatured for 4 min at 100°C. We loaded approximately 0.6 μg of total protein per lane, performed SDS-PAGE using Stain-Free™ gel (Bio-Rad), activated and scanned the gel (Gel-Doc EZ System, Bio-Rad) for quantification of total protein (ImageLab™, Bio-Rad), transferred to a nitrocellulose membrane (100 mA overnight), and used a commercial kit (OxiSelect STA-308; Cell Biolabs, San Diego, CA) to determine actin carbonylation (9). Accordingly, we incubated the membrane in TBS containing 20% methanol for 5 min and washed in 2 N HCl for 5 min. We incubated the membrane with DNPH (2,4-dinitrophenylhydrazine) in 2 N HCl for derivatization of the carbonyl group for 5 min. Subsequently, we washed the membrane in 2 N HCl 3 × 5 min and TBS containing 50% methanol 5 × 5 min. We blocked the membrane with Odyssey Blocking Buffer (LI-COR, Lincoln, NE) for 1 hr, rinsed in TBS containing 0.1% of TWEEN®−20 (Sigma-Aldrich, St. Louis, MO) 4 × 5 min, and probed with primary antibody for DNP (2,4-dinitrophenol, 230801; Cell Biolabs, San Diego, CA) at 1:1,000 dilution. After washing steps, a secondary antibody $IRDye_{800}$ (926–32211; LI-COR, Lincoln, NE) probed the membrane at 1:20,000 dilution for 1 hr in the dark, followed by washes and membrane scan in Odyssey CLx Infrared Imaging System (LI-COR, Lincoln, NE). Afterward, we

exposed the same membrane to a primary antibody for actin (JLA20; Developmental Studies Hybridoma Bank, Iowa City, IA) at 1:1,000 dilution. After washing, we incubated the membrane with secondary antibody $IRDye_{680}$ (926–68020; LI-COR, Lincoln, NE) at 1:40,000 dilution for 1 hr in the dark. We probed for actin and DNP on the same membrane using two fluorescence channels (λ = 700 and 800 nm for secondary antibodies). We used GelBandFitter (36) and Image Studio Lite Software (Li-COR, Lincoln, NE) to quantify the optical density of proteins and determined actin carbonylation as the carbonyl signal overlapping the actin band divided by total actin (9). Actin carbonylation data are the average values of measurements in triplicate. We also quantified the abundance of myosin heavy chain based on the signal intensity of the band corresponding to 200–250 kDa of the Stain-Free gel.

Statistics

We used SigmaPlot v14.0 (Systat Software, San Jose, CA) to perform normality and equal variance tests and log-transformed non-parametric data before analysis with parametric tests. We used Prism v6 (GraphPad, La Jolla, CA) to run a two-way ANOVA with Bonferroni's posthoc test (factor 1, strain: WT vs. Nox4 KO; factor 2, surgery: Sham vs. MI). In some cases, we performed posthoc tests when the two-way ANOVA interaction p-value was greater than 0.05 (58). Because fiber cross-sectional area includes several measurements per animal, we applied a linear mixed model analysis to compare these variables among groups (SPSS v26, IBM, Armonk, NY). Where appropriate, we compared data with paired or unpaired Student's t-test as needed. We used the Mann-Whitney rank-sum test for a failed normality test and Welch's t-test in case of a failed equal variance testing. All statistics are from two-tailed tests, and we highlighted differences when $p < 0.05$. We opted to report exact p-values when feasible and follow recent recommendations for data interpretation (3, 11).

Results

We performed MI surgeries on 16 mice (WT n = 8, Nox4KO n = 8) and Sham surgeries on 10 mice (n = 5 per strain). Two WT mice died within 48 hrs of MI surgery. One Nox4KO mice assigned to the MI group had to be euthanized during surgery because of an accidental ventricular tear and excessive bleeding in the process of coronary artery ligation. All animals in the Sham group survived the duration of the study. Genotyping confirmed Nox4 knockout (Figure S1). There was no difference in infarct size between strains, and MI caused cardiac hypertrophy, evident by a ~30% increase in heart weight-to-tibial length (Table 1, Figure S2). MI caused a greater percent loss of body weight compared to Sham 72 hrs post-surgery (Table 1, Figure S3). Diaphragm Nox4 mRNA was elevated almost 80% in WT with MI but did not reach the threshold for statistical significance (in fold control: Sham = 1.00 ± 0.09, MI = 1.77 ± 0.65; p = 0.057). Nox4 mRNA was undetectable in Nox4KO mice.

Diaphragm atrophy, contractile dysfunction, and protein oxidation

Diaphragm fiber cross-sectional area (CSA) was 15% lower in Nox4KO vs WT within Sham (Figure 1B). MI decreased the overall fiber CSA by 10–20% in both WT and Nox4KO (Figure 1B). Fiber type-specific analysis (Figure 1C–E) showed that MI decreased type

IIb/x fiber CSA by 20% in both WT and Nox4KO. Type IIa fiber CSA was lower post-MI than Sham, but the surgery effect on ANOVA did not reach the threshold for statistical significance ($p = 0.056$). There was no surgery or strain effect on type I CSA. Surprisingly, Nox4KO mice showed 30–50% lower mRNA abundance for MAFbx/atrogin-1 (Figure 1F) and MuRF-1 (Figure 1G). Analysis of fiber type percentage showed higher type IIa and lower type IIb/x fibers in Nox4KO vs. WT, whereas MI did not affect fiber type distribution (Figure S4).

MI decreased maximal diaphragm specific force by 10% in both WT and Nox4KO (Figure 2A). In Nox4KO, MI decreased twitch specific force by 20% (Figure 2B). The decrease in force was accompanied by increased actin carbonylation in WT and Nox4KO MI vs. Sham (Figure 2C, D), and there were no changes in the most abundant thick (MyHC) and thin (actin) filament proteins with MI or Nox4 KO (Figure S5).

Mitochondrial proteins, respiration, and H_2O_2 emission

In WT mice, MI decreased the abundance of citrate synthase and protein subunits of the mitochondrial electron transport system (ETS) complex I-V compared to Sham (Figure 3). Nox4KO decreased the abundance of citrate synthase and subunits of ETS complexes I-V compared to WT and did not prevent the MI-induced decrease in citrate synthase and subunits of ETS complexes I and II (Figure 3B–D).

The effects of Nox4KO and MI on protein abundance of subunits of mitochondrial ETS complexes did not translate to lower mitochondrial O_2 flux (Figure 4A–D). MI had no detectable effect on diaphragm fiber JO_2 (pmol/s/μg total protein), but Nox4KO displayed higher values than WT, particularly in Sham with complex I and I+II substrates during State 3 (ADP 500 μM). The JO_2 normalized to citrate synthase abundance was higher post-MI (Figure 4E–F), with differences determined mainly by WT Sham vs. MI. Nox4KO increased the respiratory control ratio (RCR) with 500 μM ADP (RCR; JO_2 State 3-to-State 2), but there was no effect of MI on RCR (WT-Sham = 2.3 ± 0.4, WT-MI = 2.4 ± 0.3, Nox4KO-Sham = 3.0 ± 0.5, Nox4KO-MI = 3.3 ± 0.5; ANOVA strain $p < 0.001$, surgery $p = 0.388$, strain × surgery $p = 0.753$).

H_2O_2 emission

There were no differences in diaphragm JH_2O_2 (pmol/min/100 μg protein), except for complex I+II substrates in the presence of ADP with lower values in Nox4KO that did not reach statistical significance (Figure 5A–C). However, JH_2O_2 normalized to citrate synthase abundance was 50–65% higher post-MI (Figure 5D–F), independent of strains. Electron leak (JH_2O_2/JO_2) in the absence of ADP was also higher post-MI for both strains but did not reach $p < 0.05$ (Figure 5G). Nox4KO decreased the electron leak in the presence of ADP, but there were no differences between Sham and MI for both strains (Figure 5H).

Discussion

There are several novel and interesting observations in our study regarding diaphragm abnormalities and adaptations in the early phase post-MI, the impact of Nox4 knockout therein, and the role of Nox4 in diaphragm physiology: 1) Diaphragm atrophy is a crucial

component of weakness in the early phase post-MI, 2) mitochondrial respiration and H_2O_2 emission normalized to citrate synthase (~mitochondrial content) increased early post-MI, 3) Nox4 knockout did not prevent the decrease in diaphragm fiber size and specific force in the early phase post-MI, and 4) Nox4 is required for the maintenance of diaphragm mitochondrial content in healthy animals and contributes to electron leak in the presence of ADP.

Nox4 and cardiac pathophysiology in the early phase post-MI

The first 72 hrs after cardiac ischemia involves the expansion of the infarct area, and it has been defined as ‘early-stage’ (53). Then, the left ventricle goes through a wider scale of remodeling that includes compensatory left ventricular hypertrophy and fibrosis that become pathological (45), and it has been defined as late-stage (53). In the early phase post-MI, Nox4 is upregulated in the heart (38). The effect of Nox4 on cardiac remodeling and function post-MI remains controversial. Transgenic cardiomyocyte overexpression of Nox4 diminished cardiac hypertrophy and fibrosis and increased survival post-MI induced by permanent ischemia (37). In contrast, cardiomyocyte-specific or whole-body Nox4 KO lowers ROS and infarct size after MI induced by ischemia-reperfusion injury or permanent ischemia (34, 51). We observed no differences in cardiac hypertrophy and infarct size in the early phase post-MI induced by permanent ischemia. The specific role of Nox4 on cardiac responses post-MI is beyond the scope of our study, and we did not pursue the mechanisms underlying our findings. In general, the lack of difference in cardiac hypertrophy and left ventricle infarct size suggests that WT and whole-body Nox4 knockout mice in our study had similar levels of cardiac dysfunction post-MI.

Nox4, atrophy, and contractile dysfunction

Diaphragm contractile dysfunction and atrophy are potential causes of decreased maximal inspiratory pressure in patients in the initial stages post-MI (39). Contractile dysfunction has been shown in studies reporting lower maximal specific force in mouse diaphragm 72 hrs post-MI (7, 50). Our data confirm the contractile dysfunction previously reported and show pronounced diaphragm fiber atrophy, especially in type IIb/x fibers. Diaphragm fiber atrophy will cause weakness (diminished absolute force) and contribute to the loss of maximal inspiratory pressure in patients in the early phase post-MI. We examined mRNA abundance of select ‘atrophy genes’ (MAFbx/atrogin and MuRF-1) – critical determinants of diaphragm atrophy with mechanical ventilation (64), chronic heart failure (1), and COPD (40) – but were unable to detect differences induced by MI or test protein levels due to high variability and limited tissue availability. Importantly, ROS and Nox4-dependent signaling mediate skeletal muscle atrophy and contractile dysfunction (13, 21, 26). Diaphragm Nox4 mRNA was increased 72 hrs post-MI, albeit not reaching statistical significance, and we considered Nox4 as a putative source of ROS and diaphragm atrophy and contractile dysfunction based on Nox4 constitutive activity (56)

Nox4 is an essential regulator of muscle fiber size. In limb muscles, Nox4 is required for overload-induced hypertrophy (25) and regeneration/growth after injury (62). Nox4 KO prevents skeletal muscle atrophy caused by angiotensin II infusion (26) or pancreatic cancer (13). However, limb muscle fiber cross-sectional area is not different in healthy Nox4 KO

and WT mice (26, 62). In general, the diaphragm fiber cross-sectional area was 15% smaller than wild-type mice. A smaller type IIa fiber cross-sectional area, although not statistically significant, and higher percentage distribution for type IIa fiber in Nox4 KO (Figure S4B), seems to be the major determinant of lower overall diaphragm fiber cross-sectional area in Nox4 KO. Surprisingly, diaphragm from Nox4 KO mice displayed lower mRNA abundance of MAFbx/atrogin and MuRF-1. However, Nox4 KO causes insulin resistance and impairs glucose uptake in the diaphragm (42), which is a muscle highly dependent on circulating glucose for carbohydrate metabolism in mice (54). Thus, differences in insulin signaling and glucose metabolism may contribute to the smaller type IIa fiber size in Nox4 KO mice.

Elevation of ROS and protein oxidation in disease states and disuse depress diaphragm contractile function (4). Nox4 is a source of ROS in skeletal muscle (19, 52), and pharmacologic inhibition of Nox4 prevents contractile dysfunction caused by metastatic bone cancer (57). Loss of diaphragm specific force within 72 hrs post-MI is accompanied by actin oxidation (carbonylation) (7), which impairs protein function (12). These observations, along with elevated Nox4 mRNA, led us to hypothesize that Nox4-dependent ROS caused diaphragm contractile dysfunction in the early stage post-MI. Contractile dysfunction in our study was evident from decreased maximal specific force post-MI. In agreement with a previous study (7), contractile dysfunction was accompanied by increased actin carbonylation. However, Nox4 KO did not prevent the loss of maximal specific force or actin carbonylation in the early-stage post-MI. Overall, our findings suggest that Nox4-dependent ROS are not mediators of actin carbonylation and diaphragm contractile dysfunction within the first 72 hrs post-MI.

Nox4 and MI impact on mitochondrial proteins, respiration, and ROS

The inflammatory and neurohumoral milieu in the early-stage post-MI can impair mitochondrial respiration (16, 43). Abnormal mitochondrial respiration is a putative cause of diminished time to task failure when patients breathe against an inspiratory resistance in the early phase post-MI (39). MI decreased the protein abundance of citrate synthase and subunits of mitochondrial ETS complexes in our study but did not affect State 3 respiration in WT mice. In fact, $\dot{V}O_2$ normalized to citrate synthase was increased with MI in wild-type mice, which may reflect a compensatory functional adaptation to increased frequency and work of breathing post-MI (5).

The abundance of mitochondrial ETS complexes and respiration are influenced by Nox4 (2, 6, 28). Nox4 knock-down or pharmacological inhibition increases ETS complex abundance and respiration in lung fibroblasts (6) and endothelial cells (28). In contrast, Nox4 KO lowered the abundance of several ETS complexes but did not lower mitochondrial respiration in the diaphragm in our study. The MI-induced increase in ‘intrinsic mitochondria respiration’ (i.e., $\dot{V}O_2$/CS) was not evident in Nox4 KO, seemingly due to elevated values in Sham. The putative reason underlying this response is unclear and may reflect an impact of Nox4-derived ROS on diaphragm muscle mitochondrial protein function or effects on the mechanics and control of breathing. The apparent discrepancy between ETS complex subunit abundance and $\dot{V}O_2$ in our study might arise from measurements with submaximal [ADP], within a range physiologically relevant for the diaphragm (22) and

during a ‘steady-state’ condition. The decreased abundance of ETS complex subunits might compromise $\dot{J}O_2$ with maximal ADP or the kinetics with submaximal [ADP], resulting in abnormal bioenergetics that causes faster diaphragm fatigue, as seen in patients in the early-stage post-MI.

Mitochondrial ROS determines redox homeostasis in the diaphragm (65), and Nox4 has been considered a source of mitochondrial ROS (2, 46), presumably via the production of H_2O_2 (19, 63). MI increased diaphragm ‘intrinsic mitochondria H_2O_2 emission’ (i.e., $\dot{J}H_2O_2$/CS) in the absence and presence of physiological levels of ADP. Nox4KO did not exert protective effects on these responses. However, our data show that Nox4 contributes, indirectly, to diaphragm mitochondria electron leak during O_2 consumption supported by ADP. The latter is a novel observation regarding the role of Nox4 in mitochondrial function.

Limitations—The main limitation of this study is our use of a whole-body Nox4 knockout model and the impossibility of distinguishing the involvement of Nox4 from other tissues or cell types on diaphragm effects post-MI. The advantage of our approach is the insight into potential diaphragm effects of systemic pharmacological inhibition of Nox4 in the early-stage post-MI. Moreover, the quantification of Nox4 protein abundance in the diaphragm was not successful with commercially available antibodies, and we relied on Nox4 mRNA as an indicator of expression. The lack of a gold-standard measurement of mitochondrial content is also a limitation. The variability of normalized $\dot{J}O_2$ and $\dot{J}H_2O_2$ data may reflect the discrepancy between the marker of mitochondrial content we used (citrate synthase abundance) and the actual mitochondrial content. No single protein appears to be a uniform marker of mitochondrial content for normalization and assessment of ‘intrinsic’ function (35). However, citrate synthase is a reasonable estimate of content compared to the gold standard of volume density by electron microscopy in skeletal muscle (29).

Conclusions

Our study showed diaphragm contractile dysfunction and fiber atrophy within 72 hrs post-MI. These findings suggest that atrophy is a crucial determinant of diaphragm weakness that contributes to diminished maximal inspiratory pressure documented in patients in the early-stage post-MI. Myocardial infarction also lowered the abundance of mitochondrial enzymes and increased intrinsic mitochondrial respiration and ROS, findings that suggest decreased mitochondrial content (or loss of specific mitochondrial proteins) and compensatory mitochondrial maladaptation that likely contribute to diminished inspiratory muscle endurance in the initial phase post-MI. Nox4 was required for normal diaphragm fiber size, mitochondrial protein abundance, and electron leak during respiration supported by ADP. However, Nox4 knockout did not prevent any of the diaphragm abnormalities we measured in the early phase post-MI.

Supplementary Material

Refer to Web version on PubMed Central for supplementary material.

Acknowledgments

We would like to thank Deborah Morse for maintaining the colony of Nox4 knockout mice used in the study and Rachel Kelley for technical support.

Funding Sources

This study was funded by a University of Florida Research Foundation Professorship award, the American Physiological Society Giles Filley Award, University of Florida DRPD-ROF2020 grant, and NIH R01-HL130318 to L. Ferreira. T.E. Ryan was funded by NIH HL149704. AHA 20PRE35200047 funded R.A. Kumar.

References

1. Adams V, Bowen TS, Werner S, Barthel P, Amberger C, Konzer A, Graumann J, Sehr P, Lewis J, Provaznik J, Benes V, Buttner P, Gasch A, Mangner N, Witt CC, Labeit D, Linke A, and Labeit S. Small-molecule-mediated chemical knock-down of MuRF1/MuRF2 and attenuation of diaphragm dysfunction in chronic heart failure. J Cachexia Sarcopenia Muscle 10: 1102–1115, 2019. [PubMed: 31140761]
2. Ago T, Kuroda J, Pain J, Fu C, Li H, and Sadoshima J. Upregulation of Nox4 by hypertrophic stimuli promotes apoptosis and mitochondrial dysfunction in cardiac myocytes. Circ Res 106: 1253–1264, 2010. [PubMed: 20185797]
3. Amrhein V, Greenland S, and McShane B. Scientists rise up against statistical significance. Nature 567: 305–307, 2019. [PubMed: 30894741]
4. Bagni MA, Colombini B, Nocella M, Pregno C, A SC, and Rassier DE. The effects of fatigue and oxidation on contractile function of intact muscle fibers and myofibrils isolated from the mouse diaphragm. Sci Rep 9: 4422, 2019. [PubMed: 30872655]
5. Barthel P, Wensel R, Bauer A, Muller A, Wolf P, Ulm K, Huster KM, Francis DP, Malik M, and Schmidt G. Respiratory rate predicts outcome after acute myocardial infarction: a prospective cohort study. Eur Heart J 34: 1644–1650, 2013. [PubMed: 23242188]
6. Bernard K, Logsdon NJ, Miguel V, Benavides GA, Zhang J, Carter AB, Darley-Usmar VM, and Thannickal VJ. NADPH Oxidase 4 (Nox4) Suppresses Mitochondrial Biogenesis and Bioenergetics in Lung Fibroblasts via a Nuclear Factor Erythroid-derived 2-like 2 (Nrf2)-dependent Pathway. J Biol Chem 292: 3029–3038, 2017. [PubMed: 28049732]
7. Bowen TS, Mangner N, Werner S, Glaser S, Kullnick Y, Schrepper A, Doenst T, Oberbach A, Linke A, Steil L, Schuler G, and Adams V. Diaphragm muscle weakness in mice is early-onset post-myocardial infarction and associated with elevated protein oxidation. J Appl Physiol (1985) 118: 11–19, 2015.
8. Close RI. Dynamic properties of mammalian skeletal muscles. Physiol Rev 52: 129–197, 1972. [PubMed: 4256989]
9. Coblentz PD, Ahn B, Hayward LF, Yoo JK, Christou DD, and Ferreira LF. Small-hairpin RNA and pharmacological targeting of neutral sphingomyelinase prevent diaphragm weakness in rats with heart failure and reduced ejection fraction. Am J Physiol Lung Cell Mol Physiol 316: L679–L690, 2019. [PubMed: 30702345]
10. Cosper PF, and Leinwand LA. Myosin Heavy Chain is not Selectively Decreased in Murine Cancer Cachexia. Int J Cancer 130: 2722–2727, 2012. [PubMed: 21796617]
11. Curran-Everett D Evolution in statistics: P values, statistical significance, kayaks, and walking trees. Adv Physiol Educ 44: 221–224, 2020. [PubMed: 32412384]
12. Dalle-Donne I, Rossi R, Giustarini D, Gagliano N, Lusini L, Milzani A, Di Simplicio P, and Colombo R. Actin carbonylation: from a simple marker of protein oxidation to relevant signs of severe functional impairment. Free Radic Biol Med 31: 1075–1083, 2001. [PubMed: 11677040]
13. Dasgupta A, Shukla SK, Vernucci E, King RJ, Abrego J, Mulder SE, Mullen NJ, Graves G, Buettner K, Thakur R, Murthy D, Attri KS, Wang D, Chaika NV, Pacheco CG, Rai I, Engle DD, Grandgenett PM, Punsoni M, Reames BN, Teoh-Fitzgerald M, Oberley-Deegan R, Yu F, Klute KA, Hollingsworth MA, Zimmerman MC, Mehla K, Sadoshima J, Tuveson DA, and Singh PK. SIRT1-NOX4 signaling axis regulates cancer cachexia. J Exp Med 217: 2020.

14. Del Rio R, Marcus NJ, and Schultz HD. Carotid chemoreceptor ablation improves survival in heart failure: rescuing autonomic control of cardiorespiratory function. J Am Coll Cardiol 62: 2422–2430, 2013. [PubMed: 24013056]
15. Dempsey JA, Romer L, Rodman J, Miller J, and Smith C. Consequences of exercise-induced respiratory muscle work. Respir Physiol Neurobiol 151: 242–250, 2006. [PubMed: 16616716]
16. Dikalov SI, and Nazarewicz RR. Angiotensin II-induced production of mitochondrial reactive oxygen species: potential mechanisms and relevance for cardiovascular disease. Antioxid Redox Signal 19: 1085–1094, 2013. [PubMed: 22443458]
17. Du XJ, Cox HS, Dart AM, and Esler MD. Sympathetic activation triggers ventricular arrhythmias in rat heart with chronic infarction and failure. Cardiovascular research 43: 919–929, 1999. [PubMed: 10615419]
18. Emde B, Heinen A, Godecke A, and Bottermann K. Wheat germ agglutinin staining as a suitable method for detection and quantification of fibrosis in cardiac tissue after myocardial infarction. Eur J Histochem 58: 2448, 2014. [PubMed: 25578975]
19. Ferreira LF, and Laitano O. Regulation of NADPH oxidases in skeletal muscle. Free Radic Biol Med 98: 18–28, 2016. [PubMed: 27184955]
20. Forrester SJ, Kikuchi DS, Hernandes MS, Xu Q, and Griendling KK. Reactive Oxygen Species in Metabolic and Inflammatory Signaling. Circ Res 122: 877–902, 2018. [PubMed: 29700084]
21. Griendling KK, Minieri CA, Ollerenshaw JD, and Alexander RW. Angiotensin II stimulates NADH and NADPH oxidase activity in cultured vascular smooth muscle cells. Circ Res 74: 1141–1148, 1994. [PubMed: 8187280]
22. Hahn D, Kumar RA, Ryan TE, and Ferreira LF. Mitochondrial Respiration and H2O2 Emission in Saponin-permeabilized Murine Diaphragm Fibers: Optimization of Fiber Separation and Comparison to Limb Muscle. Am J Physiol Cell Physiol 2019.
23. Hood DA, Memme JM, Oliveira AN, and Triolo M. Maintenance of Skeletal Muscle Mitochondria in Health, Exercise, and Aging. Annu Rev Physiol 81: 19–41, 2019. [PubMed: 30216742]
24. Ibanez B, Heusch G, Ovize M, and Van de Werf F. Evolving therapies for myocardial ischemia/reperfusion injury. J Am Coll Cardiol 65: 1454–1471, 2015. [PubMed: 25857912]
25. Ito N, Ruegg UT, Kudo A, Miyagoe-Suzuki Y, and Takeda S. Activation of calcium signaling through Trpv1 by nNOS and peroxynitrite as a key trigger of skeletal muscle hypertrophy. Nat Med 19: 101–106, 2013. [PubMed: 23202294]
26. Kadoguchi T, Shimada K, Koide H, Miyazaki T, Shiozawa T, Takahashi S, Aikawa T, Ouchi S, Kitamura K, Sugita Y, Hamad AS, Kunimoto M, Sato-Okabayashi Y, Akita K, Isoda K, and Daida H. Possible Role of NADPH Oxidase 4 in Angiotensin II-Induced Muscle Wasting in Mice. Front Physiol 9: 2018.
27. Kelley RC, and Ferreira LF. Diaphragm abnormalities in heart failure and aging: mechanisms and integration of cardiovascular and respiratory pathophysiology. Heart Fail Rev 22: 191–207, 2017. [PubMed: 27000754]
28. Koziel R, Pircher H, Kratochwil M, Lener B, Hermann M, Dencher NA, and Jansen-Durr P. Mitochondrial respiratory chain complex I is inactivated by NADPH oxidase Nox4. Biochem J 452: 231–239, 2013. [PubMed: 23514110]
29. Larsen S, Nielsen J, Hansen CN, Nielsen LB, Wibrand F, Stride N, Schroder HD, Boushel R, Helge JW, Dela F, and Hey-Mogensen M. Biomarkers of mitochondrial content in skeletal muscle of healthy young human subjects. J Physiol 590: 3349–3360, 2012. [PubMed: 22586215]
30. Leenen FH, Skarda V, Yuan B, and White R. Changes in cardiac ANG II postmyocardial infarction in rats: effects of nephrectomy and ACE inhibitors. The American journal of physiology 276: H317–325, 1999. [PubMed: 9887046]
31. Liu Q, Chen D, Wang Y, Zhao X, and Zheng Y. Cardiac autonomic nerve distribution and arrhythmia. Neural Regen Res 7: 2834–2841, 2012. [PubMed: 25317134]
32. Manea A, Tanase LI, Raicu M, and Simionescu M. Transcriptional regulation of NADPH oxidase isoforms, Nox1 and Nox4, by nuclear factor-kappaB in human aortic smooth muscle cells. Biochem Biophys Res Commun 396: 901–907, 2010. [PubMed: 20457132]
33. Marchant DJ, Boyd JH, Lin DC, Granville DJ, Garmaroudi FS, and McManus BM. Inflammation in myocardial diseases. Circ Res 110: 126–144, 2012. [PubMed: 22223210]

34. Matsushima S, Kuroda J, Ago T, Zhai P, Ikeda Y, Oka S, Fong GH, Tian R, and Sadoshima J. Broad suppression of NADPH oxidase activity exacerbates ischemia/reperfusion injury through inadvertent downregulation of hypoxia-inducible factor-1alpha and upregulation of peroxisome proliferator-activated receptor-alpha. Circ Res 112: 1135–1149, 2013. [PubMed: 23476056]
35. McLaughlin KL, Hagen JT, Coalson HS, Nelson MAM, Kew KA, Wooten AR, and Fisher-Wellman KH. Novel approach to quantify mitochondrial content and intrinsic bioenergetic efficiency across organs. Sci Rep 10: 17599, 2020.
36. Mitov MI, Greaser ML, and Campbell KS. GelBandFitter--a computer program for analysis of closely spaced electrophoretic and immunoblotted bands. Electrophoresis 30: 848–851, 2009. [PubMed: 19197901]
37. Mongue-Din H, Patel AS, Looi YH, Grieve DJ, Anilkumar N, Sirker A, Dong X, Brewer AC, Zhang M, Smith A, and Shah AM. NADPH Oxidase-4 Driven Cardiac Macrophage Polarization Protects Against Myocardial Infarction-Induced Remodeling. JACC Basic Transl Sci 2: 688–698, 2017. [PubMed: 29445778]
38. Murdoch CE, Zhang M, Cave AC, and Shah AM. NADPH oxidase-dependent redox signalling in cardiac hypertrophy, remodelling and failure. Cardiovascular research 71: 208–215, 2006. [PubMed: 16631149]
39. Neves LM, Karsten M, Neves VR, Beltrame T, Borghi-Silva A, and Catai AM. Relationship between inspiratory muscle capacity and peak exercise tolerance in patients post-myocardial infarction. Heart Lung 41: 137–145, 2012. [PubMed: 22177761]
40. Ottenheijm CA, Heunks LM, Li YP, Jin B, Minnaard R, van Hees HW, and Dekhuijzen PN. Activation of the ubiquitin-proteasome pathway in the diaphragm in chronic obstructive pulmonary disease. American journal of respiratory and critical care medicine 174: 997–1002, 2006. [PubMed: 16917114]
41. Perry CG, Kane DA, Lin CT, Kozy R, Cathey BL, Lark DS, Kane CL, Brophy PM, Gavin TP, Anderson EJ, and Neufer PD. Inhibiting myosin-ATPase reveals a dynamic range of mitochondrial respiratory control in skeletal muscle. Biochem J 437: 215–222, 2011. [PubMed: 21554250]
42. Plecita-Hlavata L, Jaburek M, Holendova B, Tauber J, Pavluch V, Berkova Z, Cahova M, Schroder K, Brandes RP, Siemen D, and Jezek P. Glucose-Stimulated Insulin Secretion Fundamentally Requires H2O2 Signaling by NADPH Oxidase 4. Diabetes 69: 1341–1354, 2020. [PubMed: 32245800]
43. Reid MB, and Li YP. Tumor necrosis factor-alpha and muscle wasting: a cellular perspective. Respir Res 2: 269–272, 2001. [PubMed: 11686894]
44. Roberts BM, Frye GS, Ahn B, Ferreira LF, and Judge AR. Cancer cachexia decreases specific force and accelerates fatigue in limb muscle. Biochem Biophys Res Commun 435: 488–492, 2013. [PubMed: 23673294]
45. Rubin SA, Fishbein MC, and Swan HJ. Compensatory hypertrophy in the heart after myocardial infarction in the rat. J Am Coll Cardiol 1: 1435–1441, 1983. [PubMed: 6222102]
46. Sakellariou GK, Vasilaki A, Palomero J, Kayani A, Zibrik L, McArdle A, and Jackson MJ. Studies of mitochondrial and nonmitochondrial sources implicate nicotinamide adenine dinucleotide phosphate oxidase(s) in the increased skeletal muscle superoxide generation that occurs during contractile activity. Antioxid Redox Signal 18: 603–621, 2013. [PubMed: 23050834]
47. Schroder K, Zhang M, Benkhoff S, Mieth A, Pliquett R, Kosowski J, Kruse C, Luedike P, Michaelis UR, Weissmann N, Dimmeler S, Shah AM, and Brandes RP. Nox4 is a protective reactive oxygen species generating vascular NADPH oxidase. Circulation research 110: 1217–1225, 2012. [PubMed: 22456182]
48. Sieck GC, Ferreira LF, Reid MB, and Mantilla CB. Mechanical properties of respiratory muscles. Compr Physiol 3: 1553–1567, 2013. [PubMed: 24265238]
49. Sieck GC, and Fournier M. Diaphragm motor unit recruitment during ventilatory and nonventilatory behaviors. J Appl Physiol (1985) 66: 2539–2545, 1989. [PubMed: 2745316]
50. Smith IJ, Roberts B, Beharry A, Godinez GL, Payan DG, Kinsella TM, Judge AR, and Ferreira LF. Janus kinase inhibition prevents cancer- and myocardial infarction-mediated diaphragm muscle weakness in mice. Am J Physiol Regul Integr Comp Physiol 310: R707–710, 2016. [PubMed: 26864813]

51. Stevenson MD, Canugovi C, Vendrov AE, Hayami T, Bowles DE, Krause KH, Madamanchi NR, and Runge MS. NADPH Oxidase 4 Regulates Inflammation in Ischemic Heart Failure: Role of Soluble Epoxide Hydrolase. Antioxid Redox Signal 31: 39–58, 2019. [PubMed: 30450923]
52. Sun QA, Hess DT, Nogueira L, Yong S, Bowles DE, Eu J, Laurita KR, Meissner G, and Stamler JS. Oxygen-coupled redox regulation of the skeletal muscle ryanodine receptor-Ca2+ release channel by NADPH oxidase 4. Proc Natl Acad Sci U S A 108: 16098–16103, 2011. [PubMed: 21896730]
53. Sutton MG, and Sharpe N. Left ventricular remodeling after myocardial infarction: pathophysiology and therapy. Circulation 101: 2981–2988, 2000. [PubMed: 10869273]
54. TeSlaa T, Bartman CR, Jankowski CSR, Zhang Z, Xu X, Xing X, Wang L, Lu W, Hui S, and Rabinowitz JD. The Source of Glycolytic Intermediates in Mammalian Tissues. Cell metabolism 33: 367–378 e365, 2021. [PubMed: 33472024]
55. van Hees HW, van der Heijden HF, Ottenheijm CA, Heunks LM, Pigmans CJ, Verheugt FW, Brouwer RM, and Dekhuijzen PN. Diaphragm single-fiber weakness and loss of myosin in congestive heart failure rats. Am J Physiol Heart Circ Physiol 293: H819–828, 2007. [PubMed: 17449557]
56. von Lohneysen K, Noack D, Hayes P, Friedman JS, and Knaus UG. Constitutive NADPH oxidase 4 activity resides in the composition of the B-loop and the penultimate C terminus. The Journal of biological chemistry 287: 8737–8745, 2012. [PubMed: 22277655]
57. Waning DL, Mohammad KS, Reiken S, Xie W, Andersson DC, John S, Chiechi A, Wright LE, Umanskaya A, Niewolna M, Trivedi T, Charkhzarrin S, Khatiwada P, Wronska A, Haynes A, Benassi MS, Witzmann FA, Zhen G, Wang X, Cao X, Roodman GD, Marks AR, and Guise TA. Excess TGF-beta mediates muscle weakness associated with bone metastases in mice. Nat Med 21: 1262–1271, 2015. [PubMed: 26457758]
58. Wei J, Carroll RJ, Harden KK, and Wu G. Comparisons of treatment means when factors do not interact in two-factorial studies. Amino Acids 42: 2031–2035, 2012. [PubMed: 21547361]
59. Wen Y, Murach KA, Vechetti IJ Jr., Fry CS, Vickery C, Peterson CA, McCarthy JJ, and Campbell KS. MyoVision: software for automated high-content analysis of skeletal muscle immunohistochemistry. Journal of applied physiology 124: 40–51, 2018. [PubMed: 28982947]
60. Woods PR, Olson TP, Frantz RP, and Johnson BD. Causes of breathing inefficiency during exercise in heart failure. J Card Fail 16: 835–842, 2010. [PubMed: 20932466]
61. Xia F, Wang C, Jin Y, Liu Q, Meng Q, Liu K, and Sun H. Luteolin protects HUVECs from TNF-alpha-induced oxidative stress and inflammation via its effects on the Nox4/ROS-NF-kappaB and MAPK pathways. J Atheroscler Thromb 21: 768–783, 2014. [PubMed: 24621786]
62. Youm TH, Woo SH, Kwon ES, and Park SS. NADPH Oxidase 4 Contributes to Myoblast Fusion and Skeletal Muscle Regeneration. Oxid Med Cell Longev 2019: 3585390, 2019.
63. Zhang M, Brewer AC, Schroder K, Santos CX, Grieve DJ, Wang M, Anilkumar N, Yu B, Dong X, Walker SJ, Brandes RP, and Shah AM. NADPH oxidase-4 mediates protection against chronic load-induced stress in mouse hearts by enhancing angiogenesis. Proc Natl Acad Sci U S A 107: 18121–18126, 2010. [PubMed: 20921387]
64. Zhu E, Sassoon CS, Nelson R, Pham HT, Zhu L, Baker MJ, and Caiozzo VJ. Early effects of mechanical ventilation on isotonic contractile properties and MAF-box gene expression in the diaphragm. J Appl Physiol (1985) 99: 747–756, 2005. [PubMed: 15831803]
65. Zuo L, Best TM, Roberts WJ, Diaz PT, and Wagner PD. Characterization of reactive oxygen species in diaphragm. Acta Physiol (Oxf) 213: 700–710, 2015. [PubMed: 25330121]

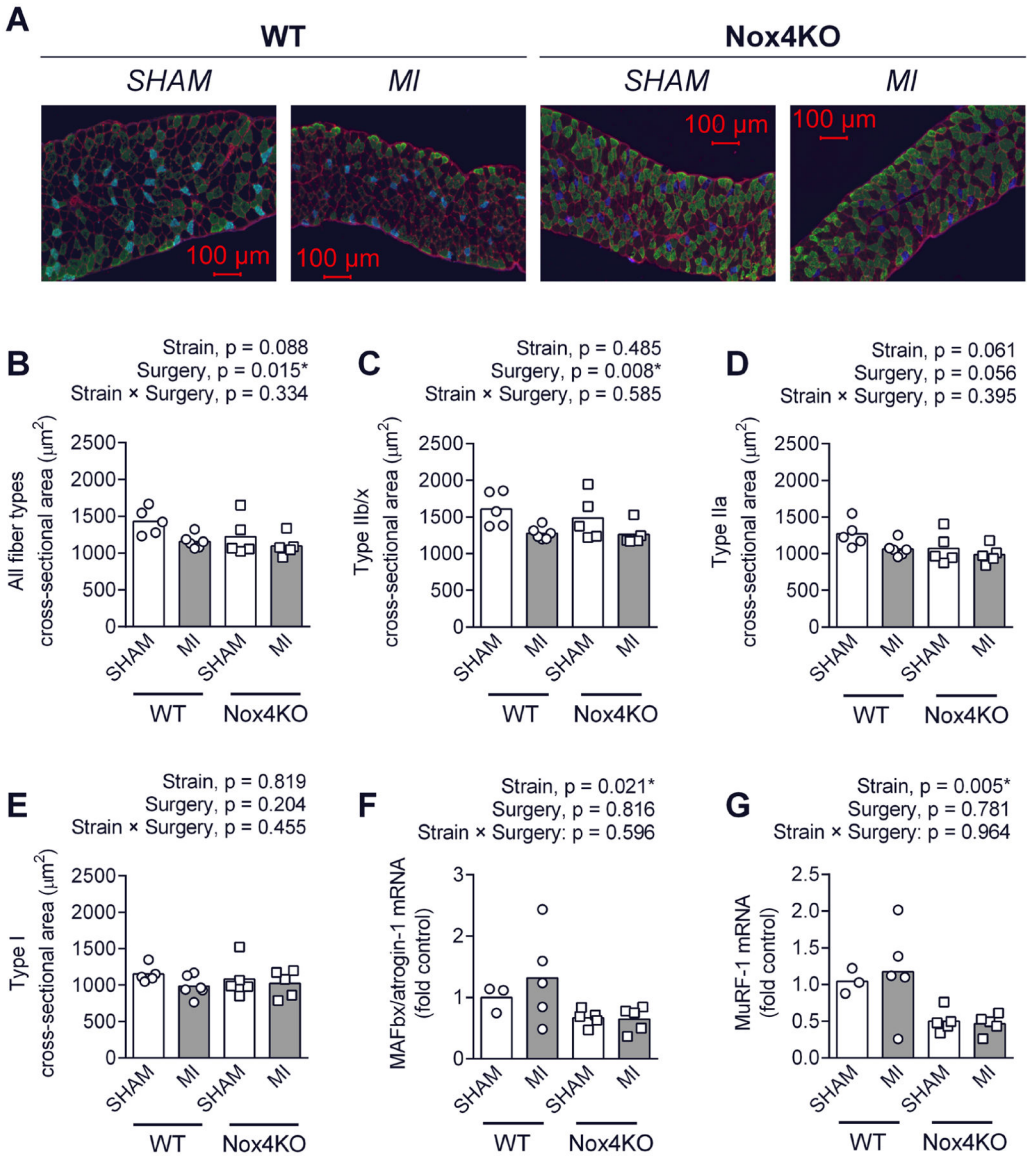

Figure 1.

Diaphragm morphology and ubiquitin ligase mRNA. (A) Representative images of transverse cross-sections of the diaphragm (blue: type I, green: type IIa, black: type IIb/x, red: connective tissue). (B-E) Fiber cross-sectional area. (F, G) mRNA levels of MAFbx/atrogin-1 and MuRF-1. Data are fold-control relative to WT-Sham. Bars are mean values. N = 3–6 mice/group. Statistical analysis by linear mixed model (B-E) and two-way ANOVA (F, G) with Bonferroni post-hoc test. * $p < 0.05$.

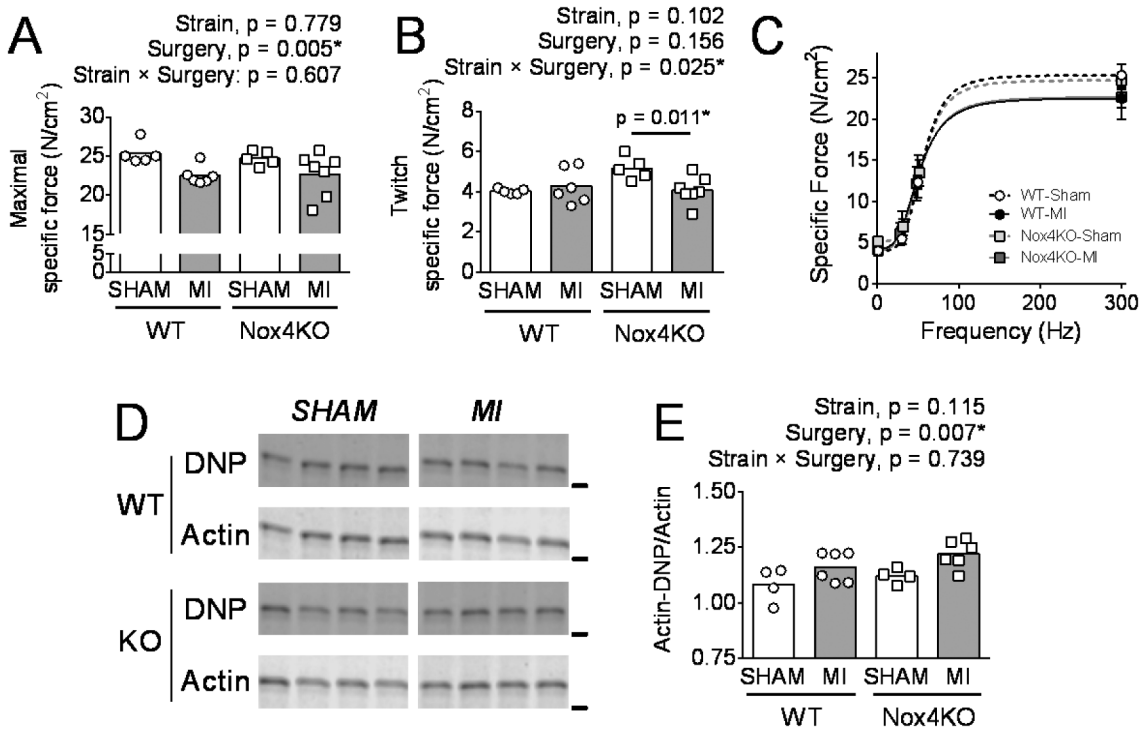

Figure 2.

Diaphragm isometric forces and actin carbonylation. (A) Maximal specific force (N/cm^2), (B) Twitch specific force (N/cm^2), (C) Specific force-frequency relationship, (D) Immunoblots of carbonylated actin (DNP: 2,4-dinitrophenol) and actin (horizontal bars ~37 kDa). (E) Optical density band corresponding to actin (DNP) normalized to actin signal in Western Blot image. Bars show mean values. N = 4–7 mice/group. Statistical analysis by two-way ANOVA and Bonferroni post-hoc test. *$p < 0.05$.

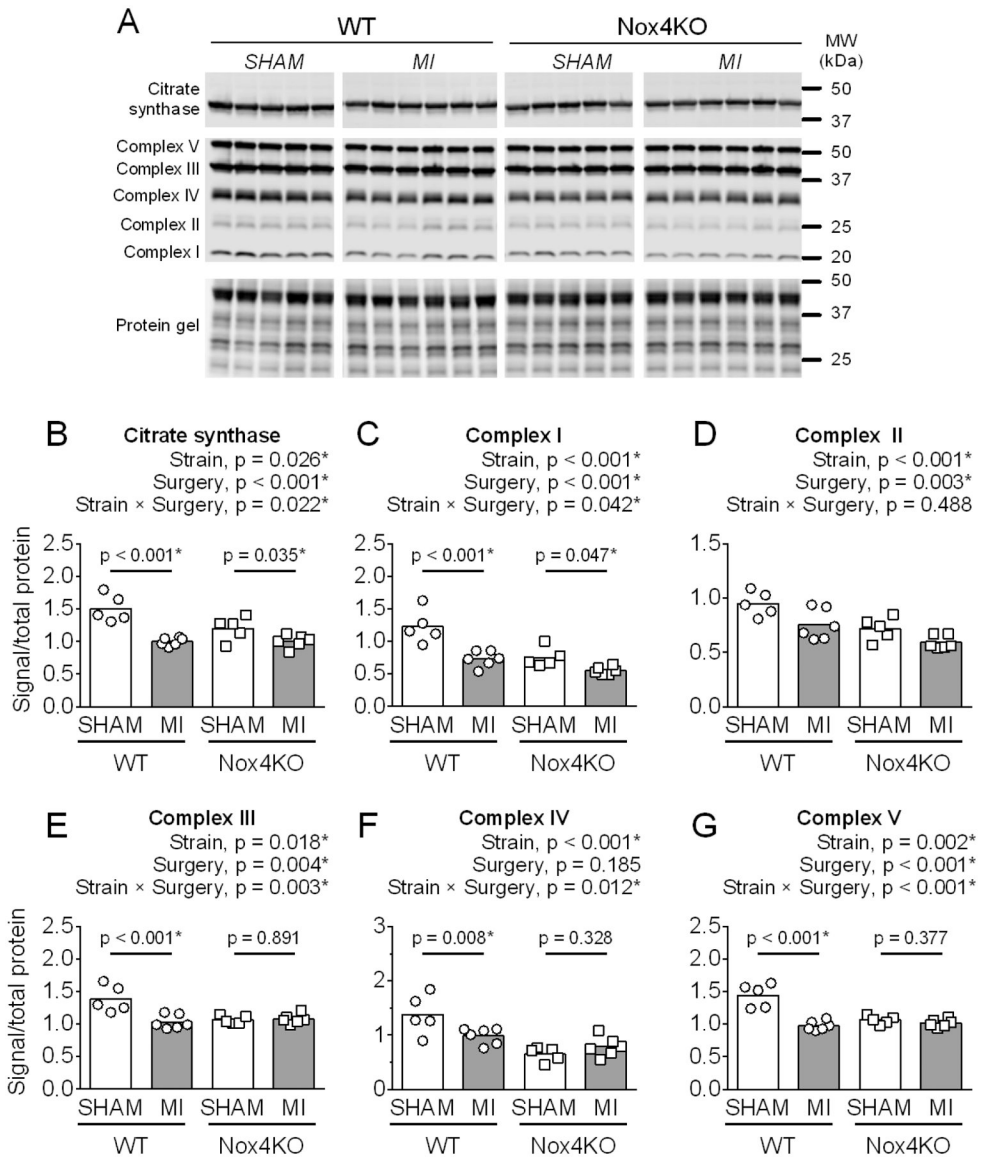

Figure 3.

Diaphragm mitochondrial protein abundance. (A) Immunoblots of citrate synthase (top), mitochondrial ETS complexes I-V subunits (middle), and representative region of total protein gel (bottom). Approximate molecular weights (MW) shown by horizontal dashed lines. (B-F) Quantification of immunoblot optical density normalized to total protein signal from each lane. Bars show mean values. N = 5–6 mice/group. Statistical analysis by two-way ANOVA and Bonferroni post-hoc test. *p < 0.05.

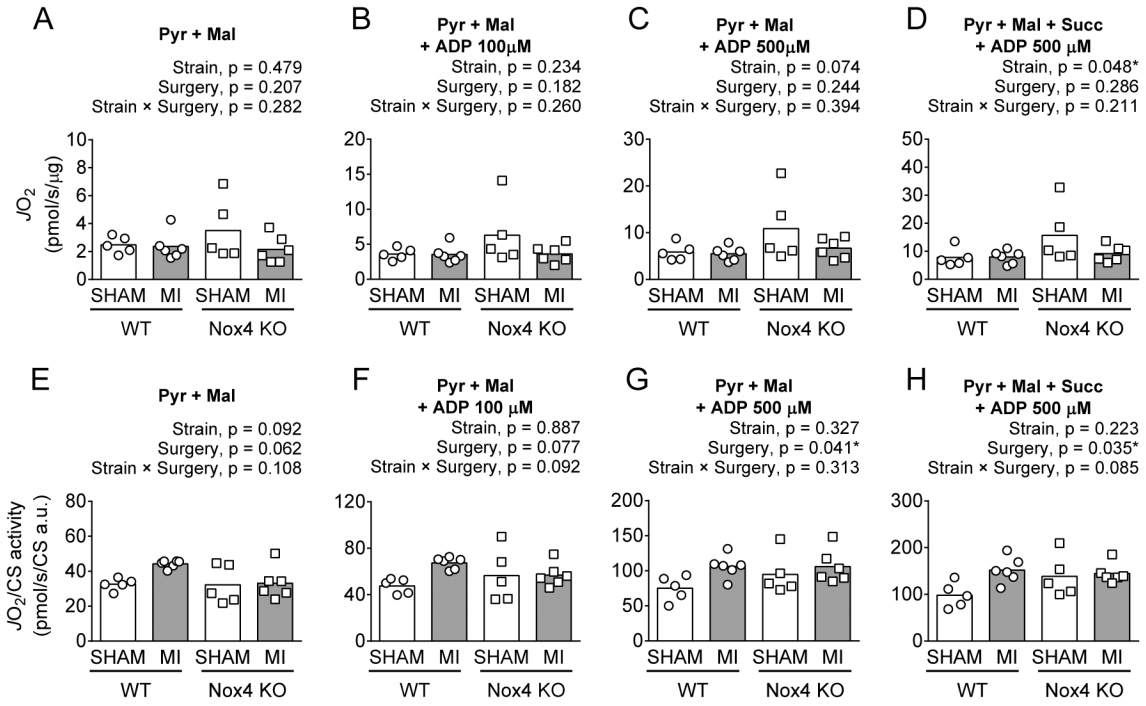

Figure 4.

Oxygen consumption rate (JO_2) from permeabilized diaphragm fiber bundle with substrates for complex I, II and ADP. (A-D) JO_2 normalized to fiber bundle protein content (JO_2: pmol/s/μg). (E-H) JO_2 normalized to fiber bundle citrate synthase abundance (JO_2/CS: pmol/s/CS a.u.), where a.u. is arbitrary unit. Bars show group mean. N = 5–6 mice/group. Statistical analysis by two-way ANOVA. *$p < 0.05$. Panels E and F: Student t-test showed $p < 0.001$ for Wildtype Sham vs MI, but no statistically significant difference between Nox4KO Sham and MI.

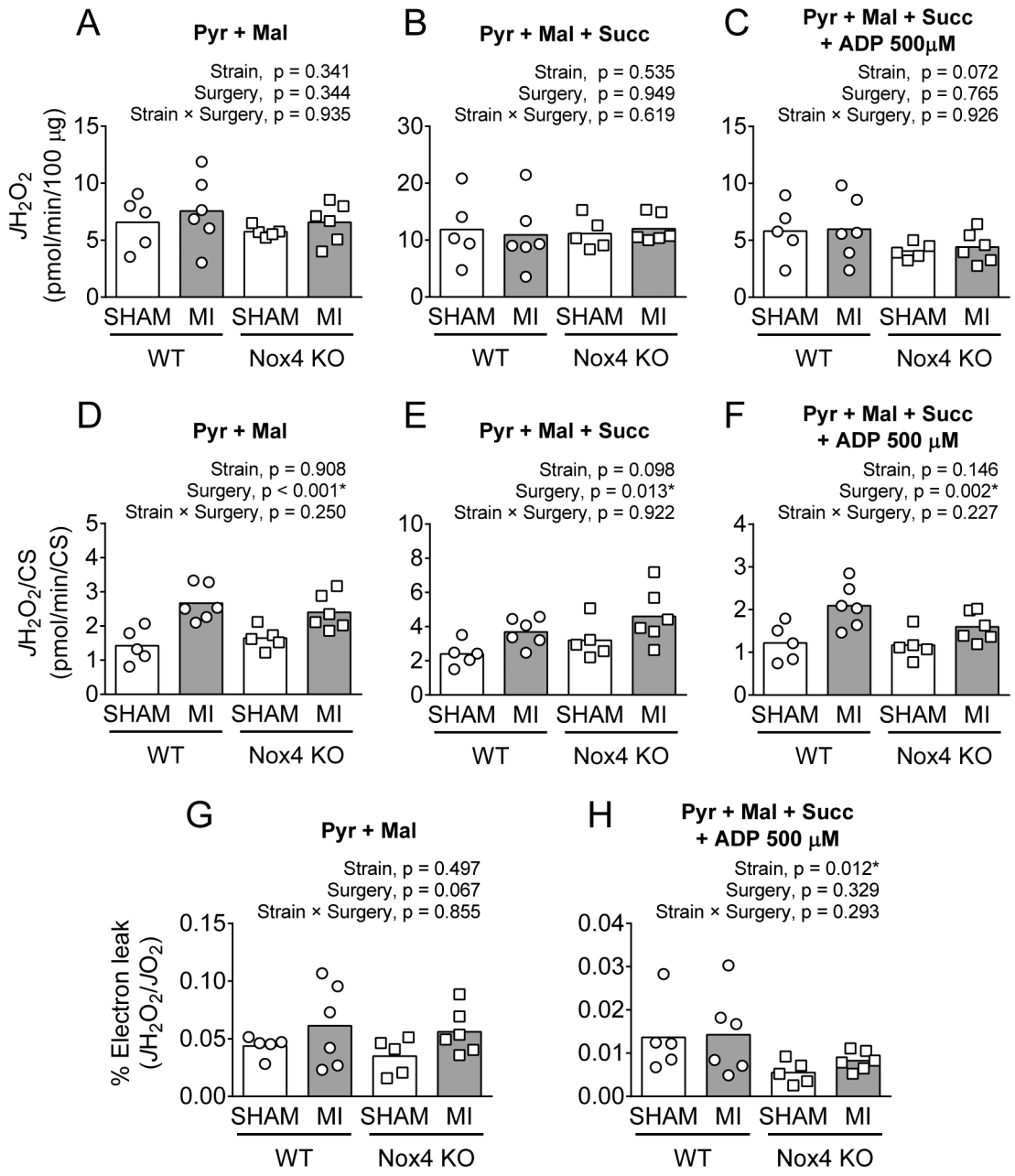

Figure 5.

Hydrogen peroxide emission rate ($J_{H_2O_2}$) from the permeabilized diaphragm fiber bundle with substrates for complex I, II and ADP. (A-C) $J_{H_2O_2}$ normalized to total protein content of the fiber bundle ($J_{H_2O_2}$: pmol/min/100 µg total protein). (D-F) $J_{H_2O_2}$ normalized to citrate synthase content of the fiber bundle ($J_{H_2O_2}$/CS: pmol/min/CS). (G, H) % Electron leak ($J_{H_2O_2}/J_{O_2}$) by parallel measurements of O_2 consumption rates and H_2O_2 emission rates. Bars show group mean. N = 5–6 mice/group. Statistical analysis by two-way ANOVA. *p < 0.05.

Table 1.

Animal characteristics

	WT (C57BL6/J)		Nox4KO		p-value		
	Sham (n = 5)	**MI (n = 6)**	**Sham (n = 5)**	**MI (n = 7)**	**Strain**	**Surgery**	**Strain × Surgery**
Body weight – pre (g)	34 ± 3	34 ± 1	30 ± 2	34 ± 2	0.033 *	0.045 *	0.062
Body weight – post (g)	33 ± 2	32 ± 2	29 ± 2	30 ± 2	0.011 *	0.722	0.174
ΔBody weight (%)	−4 ± 5	−10 ± 6	−5 ± 5	−10 ± 4	0.232	0.032 *	0.743
Heart weight (HW, g)	133 ± 12	184 ± 19	113 ± 7	150 ± 11	< 0.001 *	< 0.001 *	0.231
HW/TL (mg/mm)	7.5 ± 0.8	10.2 ± 1.1	6.5 ± 3	8.6 ± 0.7	0.001 *	< 0.001 *	0.391
Infarct size (%)	-	55 ± 11	-	59 ± 11		0.342	

Each row contains p-values from two-way ANOVA for each factor and interaction for body weight, heart weight analysis. We performed unpaired Student's t-test for infarct size in MI WT vs. Nox4 KO. HW, heart weight; TL, tibial length. Data are means ± SD.

* $p < 0.05$ by two-way ANOVA.